Spiral-In/Out BOLD fMRI for Increased SNR and Reduced Susceptibility Artifacts

Gary H. Glover* and Christine S. Law

BOLD fMRI is hampered by dropout of signal in the orbitofrontal and parietal brain regions due to magnetic field gradients near air-tissue interfaces. This work reports the use of spiral-in trajectories that begin at the edge of *k*-space and end at the origin, and spiral in/out trajectories in which a spiral-in readout is followed by a conventional spiral-out trajectory. The spiral-in trajectory reduces the dropout and increases the BOLD contrast. The spiral-in and spiral-out images can be combined in several ways to simultaneously achieve increased signal-to-noise ratio (SNR) and reduced dropout artifacts. Activation experiments employing an olfaction task demonstrate significantly increased activation volumes due to reduced dropout, and overall increased SNR in all regions.   Magn Reson Med 46: 515–522, 2001. © 2001 Wiley-Liss, Inc.

The most widely used form of fMRI exploits BOLD contrast (1,2) to produce maps of neuronal activation. When the transverse magnetization decay is exponential, changes in BOLD contrast are maximized if the echo time (TE) is made equal to the susceptibility-mediated transverse relaxation time constant, T_2^*. In uniform brain the T_2^* for gray matter is about 50 ms at 3T (3,4); thus, in sensitizing the acquisition to BOLD changes from the microscopic gradients surrounding capillaries, the acquisition is also made exquisitely sensitive to intravoxel dephasing resulting from macroscopic field gradients established near air-tissue interfaces. These susceptibility-induced field gradients (SFGs) cause severe dropout of signal in the frontal orbital and lateral parietal brain regions due to the difference in magnetic susceptibility of tissue and air (~ -8 ppm). These dropouts can limit the applicability of fMRI for many cognitive experiments.

Several methods have been proposed to reduce the effect of SFGs. One class of techniques corrects for dropouts caused when SFGs shift the center of excitation *k*-space (k_z direction), by applying compensation gradients in the slice-selection direction to refocus the dephased spins (5,6). 3D compensation schemes were introduced by Yang et al. (7,8) in which multiple echoes and Fourier inversion are used to create compensated images, and by Glover (9), who used extended coverage of k_z-space with windowed reconstruction to provide efficiency improvements in gathering the compensated images. A related method simply decreases the

slice thickness and averages adjacent slices (10,11). However, each of these methods suffers from prolonged scan time and loss of SNR efficiency. Another class of methods uses tailored RF pulses to compensate the dephasing during excitation (12–14). The design of these pulses is complex and ideally must be tailored for each subject, and their effectiveness is reduced by gradient system limitations that cause the pulses to be lengthy. In addition, all of these compensation methods are effective only for SFGs in the slice-select direction, and they provide no mitigation for intravoxel dephasing caused by in-plane gradients.

Spiral methods have several advantages over other techniques for fMRI applications, including low sensitivity to brain motion and efficient gradient utilization, which in turn leads to shorter acquisition windows (15). One potential disadvantage relative to EPI methods, however, is that the spiral readout starts at TE, and all higher spatial frequency components are gathered at longer evolution times. This attenuates the higher frequencies for regions near SFGs and can cause loss of signal if the effective T_2^* is short compared to TE. Single-shot EPI methods usually gather half of the *k*-space data on either side of TE, and thus the loss of high frequencies near the end of the readout is partially compensated for by the accentuated components near the beginning, even though the total EPI readout duration is longer. Nevertheless, the advantages of spiral methods provide impetus for further exploration of means to decrease the signal loss due to SFGs. Bornert et al. (16) introduced the concept of reversed spirals with an eye to improving TR efficiency, but did not discuss the issues of signal dropout.

In this work we explore the use of spiral-in and spiral in/out trajectories for improved BOLD contrast in regions near SFGs. Since the spatial extent of cortical regions is generally a very small fraction of the imaging field of view (FOV), the *k*-space representation of activated regions is extensive, and the high frequencies are important for their depiction. Therefore, the spiral-in trajectory has potential because the entire acquisition window occurs before TE instead of after it, and should provide increased signal for the higher spatial frequencies rather than attenuation. However, once a spiral-in acquisition has concluded, a spiral-out readout can be performed in the same acquisition, and the two sets of images can be combined to further improve the SNR. In this case, it is necessary to examine whether the spiral-out image is compromised by motion noise arising from the additional gradient moments of the preceding spiral-in trajectory.

MATERIALS AND METHODS

Theory

When the acquisition window (Tad) is short compared to T_2^*, the image has T_2^* weighting defined by the intensity at

---

Department of Radiology, Center for Advanced MR Technology, Stanford University School of Medicine, Stanford, California.

*Correspondence to: Gary H. Glover, Ph.D., Stanford University School of Medicine, Department of Diagnostic Radiology, Lucas MR Center, Stanford, CA 94305-5488. E-mail: gary@s-word.stanford.edu
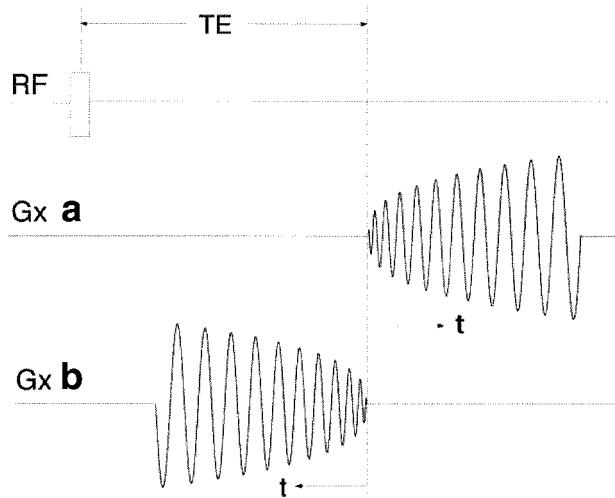
FIG. 1. (a) Spiral-out and (b) spiral-in pulse sequences, showing only x readout gradients. Each readout starts at TE ($t = 0$) and has duration Tad. High spatial frequencies are accentuated for spiral-in trajectory, and attenuated for conventional spiral-out case due to T_2^* decay.

which the trajectory intersects the k-space origin, i.e., the TE. However, when Tad is comparable to T_2^*, the weighting of the separate components of k-space must be accounted for (17), and the effective weighting depends on the k-space spectrum of the object being imaged. Blurring due to off-resonance effects has been studied for conventional spiral-out methods (18). Here, we consider the effect of T_2^* decay for spiral-out and spiral-in trajectories, as shown in Fig. 1.

Assume that a brain region can be simulated as a 2D homogeneous object with the Gaussian profile centered at the origin, having $R_2^* = 1/T_2^*$. Furthermore, assume for simplicity that a dephasing SFG b(x) is directed only along

the x axis with linear gradient amplitude g, so that b = gx. Measurements are obtained with single-shot, slew-rate limited spiral-in and spiral-out readouts (19). Then, the reconstructed image intensity at the origin I_o is (see Appendix):

$$I_0 = e^{-TE\,R_2^*} \left| \int_0^1 Q_\pm(\tau)\,d\tau \right|, \qquad [1]$$

where $Q_\pm$ is defined in the appendix, the positive sign is chosen for spiral-out and the negative sign is chosen for spiral-in. The BOLD response B is proportional to $\partial I_o/\partial R_2^*$. Then,

$$B = e^{-TE\,R_2^*} \left| TE \int_0^1 Q_\pm(\tau)\,d\tau \pm Tad \int_0^1 \tau Q_\pm(\tau)\,d\tau \right|. \qquad [2]$$

Equations [1] and [2] were evaluated as a function of TE for various values of object radius a and SFG amplitude g, using parameters typical for fMRI: D = 24 cm, p = 3.75 mm, and gradient slew rate of 190 T/m/s. T_2^* was assumed to be 50 ms. The raw image intensity and BOLD sensitivity were compared for spiral-out and spiral-in trajectories. Results for an object with a 15-cm diameter (representing a head) and a 1.5-cm diameter are shown in Fig. 2.

For the large object (top plots, Fig. 2a and b), when g = 0 the raw signal falls off exponentially for both trajectories, and the BOLD sensitivity B peaks at TE = T_2^* (plots denoted with 0). This is expected because the spectral content of the object is concentrated near the k-space origin, which is sampled when t = 0 (i.e., at TE), and thus the finite width of the readout Tad does not come into play. For finite g, the spiral-in trajectory has increased raw sig-
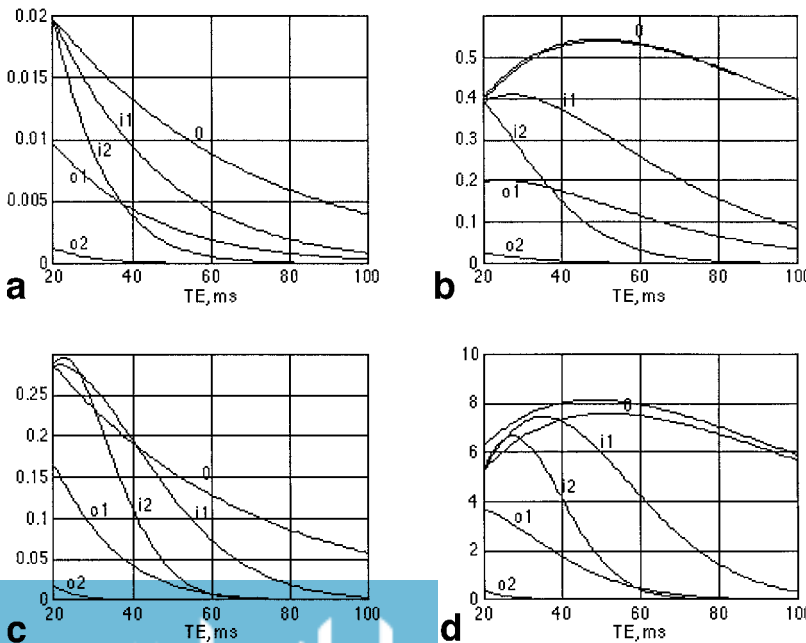

FIG. 2. Calculated MR intensity (left) and BOLD contrast (right) for a uniform object (a and b) 15 cm or (c and d) 1.5 cm in diameter as a function of TE, with three levels of dephasing gradients and other parameters given in the text. The solid and dashed lines are for spiral-out and spiral-in trajectories, respectively, and ordinate units are arbitrary. a and b: 0 = no SFG, 1 = SFG of 0.03 mG/cm, and 2 = SFG of 0.1 mG/cm. c and d: 0 = no SFG, 1 = SFG of 1.0 mG/cm, and 2 = SFG of 2.0 mG/cm. The raw amplitudes are nearly the same for spiral-in vs. spiral-out when there is no dephasing, although some difference is observed in the corresponding BOLD plots. With SFGs, the spiral-in trajectory has greater signal and BOLD contrast.

Table 1
Activation Volumes and SFNR

	Subject 1	Subject 2	Subject 3	Subject 4	Subject 5	Normalized average
Spiral-out						
Act. vol.	14 (1.00)	6 (1.00)	50 (1.00)	15 (1.00)	4 (1.00)	1.00
SFNR	108 (1.00)	104 (1.00)	116 (1.00)	53 (1.00)	74 (1.00)	1.00
Spiral-in						
Act. vol.	70 (5.00)	6 (1.00)	0	36 (2.40)	6 (1.50)	1.98 ± 1.70
SFNR	103 (0.95)	98 (0.94)	127 (0.95)	56 (1.06)	80 (1.08)	1.00 ± 0.06
Spiral-in (in/out)						
Act. vol.	70 (5.00)	14 (2.33)	27 (0.54)	28 (1.87)	6 (1.50)	2.25 ± 1.50
SFNR	96 (0.89)	108 (1.04)	115 (0.89)	58 (1.09)	79 (1.07)	1.00 ± 0.09
Spiral-out (in/out)						
Act. vol.	49 (3.50)	0	66 (1.32)	20 (1.25)	2 (0.50)	1.51 ± 1.03
SFNR	103 (0.95)	92 (0.88)	127 (0.95)	57 (1.08)	76 (1.03)	0.98 ± 0.07
Average combination						
Act. vol.	107 (7.64)	13 (2.17)	118 (2.36)	40 (2.67)	20 (5.00)	3.97 ± 2.10
SFNR	119 (1.10)	135 (1.30)	156 (1.10)	72 (1.36)	103 (1.39)	1.25 ± 0.13
Weighted combination						
Act. vol.	108 (7.71)	14 (2.33)	125 (2.50)	39 (2.60)	23 (5.75)	4.18 ± 2.18
SFNR	123 (1.14)	135 (1.30)	157 (1.35)	71 (1.34)	103 (1.39)	1.30 ± 0.09

nal and BOLD contrast (i1, i2) vs. those for the spiral-out trajectory (o1, o2).

For the smaller object (Fig. 2c and d), when g = 0 the raw signal is nearly exponentially reduced with increased TE, but some disparity is noted in the BOLD sensitivity between the two trajectories. In particular, the B for the spiral-out trajectory peaks when TE $< T_2^*$, while B for the spiral-in trajectory peaks for TE $> T_2^*$. This reflects the fact that the spectral content of the smaller object is distributed enough that contributions are sampled across a larger portion of Tad, and the effective peak shifts beyond the start of the readout, t > 0. As with the larger object, the spiral-in trajectory has greater signal and BOLD sensitivity than for the spiral-out trajectory when g > 0. Note that greater values of g were required in the simulations for the smaller object to show an observable effect.

These simulations were performed for a convenient but rather unrealistic case of a uniform object and linear dephasing gradient in one transverse direction. However, the results strongly suggest that the spiral-in trajectory should recover qualitatively greater signal and BOLD sensitivity when dephasing gradients are present, while not losing performance in uniform brain regions.

Experiments

Functional activation data were obtained with an olfactory task designed to elicit neuronal response in the amygdala and pyriform regions in which SFGs from the nasal passage typically create large signal dropout. By acquiring data with three trajectories (spiral-out, spiral-in, and spiral-in/out) it was possible to determine whether the spiral-in trajectory recovers additional signal in SFG-compromised regions and at least the same signal in uniform regions, whether additional SNR is obtained by combining the spiral-in and spiral-out images, and whether additional noise is induced in the spiral-out image for the combined trajectory by motion noise from the additional moments of the preceding spiral gradients.

The task was a block design in which subjects were visually instructed to sniff through the nose for 2 s every 5 s during "on" blocks of 25-s duration, and to breathe through the mouth with the same pattern during 25-s "off blocks." Six complete cycles were used, for a total scan time of 300 s. Subjects were instructed to attempt to discern an odorant during the "on" block, even though no odorant was intentionally presented. Sniffing has been shown to provide activation in the primary olfactory cortex and amygdala (20).

Five normal right-handed volunteers were scanned after they gave informed consent in accordance with a protocol approved by the Stanford Institutional Review Board. For each subject, three scans were performed using the conventional spiral-out trajectory as well as spiral-in and spiral-in/out trajectories. The order of the scans was randomized across the subjects. Breathing instructions were presented with a video projector and back projection screen mounted on the coil holder.

All imaging data were acquired with a 3T scanner equipped with high-performance gradients and receiver (GE Signa, rev 8.3, Milwaukee, WI). For four subjects (subjects 1–3, and 5 in Table 1) an in-house-made birdcage coil was used, whereas for subject 4 the GE head coil was used. T_1-weighted fast spin-echo (FSE) scans were obtained for anatomic reference (TR/TE/ETL = 68 ms/4000 ms/12). An automated high-order shimming method based on spiral acquisitions was employed to reduce B_o heterogeneity (21). Functional acquisitions used TE = 30 ms, TR = 1000 ms, flip angle = 60°, BW = ± 100 kHz, and FOV = 24 cm. Eight 5-mm slices were acquired with an oblique axial scan plane. The spiral-out trajectory was a single-shot, slew-rate limited, uniform density spiral with a matrix of 64 × 64 (19). For spiral-in, the calculated spiral-out waveforms were time reversed and negated. The spiral-in/out acquisitions used the spiral-in readout followed 100 μs later with the spiral-out readout. In this way, two separate images were obtained with nearly the same TE.

Images were reconstructed with an off-line computer (Sun Microsystems, Mountain View, CA) using gridding and FFTs. The k-space trajectory was measured with Duyn's method (22) and used for gridding the data rather than using the calculated trajectory, as artifacts resulted from the latter because of eddy currents and hysteresis. Linear shim corrections for each slice were applied during reconstruction using individual field maps obtained during the scan (18), and corrections were also performed for concomitant field effects (23).

Data Analysis

Spiral-In/Out Image Combination

The spiral-in and spiral-out data were combined for the spiral-in/out acquisition by averaging the two images frame-by-frame to obtain a new time-series. This averaging method would be expected to provide a $\sqrt{2}$ SNR advantage in uniform regions where both spiral-in and spiral-out images contribute if the noise is uncorrelated. However, the spiral-in and -out images share common data at t = 0 (the k-space origin), and thus the actual SNR advantage is expected to be less by a factor that depends on the noise autocorrelation function. On the other hand, in nonuniform, SFG-compromised regions in which the spiral-out image exhibits dropout and contributes only noise, averaging will serve to decrease the SNR. Therefore, an alternate combination method that uses a weighted average was also investigated, in which the weighting between the two images I_{in} and I_{out} for the spiral-in and spiral-out acquisitions, respectively, is determined by the intensities in the time-series average images:

$$I_{comb} = WI_{in} + (1 - W)I_{out}, \qquad [3]$$

where

$$W = \bar{I}_{in}/(\bar{I}_{in} + \bar{I}_{out}) \qquad [4]$$

in which the average images are indicated by the bars in Eq. [4]. Thus, in regions in which the spiral-out average image has lower intensity, the resultant image is weighted toward the spiral-in image, whereas in uniform regions the combination reverts to a simple average.

Activation Analysis

For each subject, the three scans yielded six separate time-series: spiral-out scan, spiral-in scan, the two separate images from the spiral-in/out scan, and the two combination methods for the spiral-in/out scan. Each was analyzed using cross-correlation with sine- and cosine-waves (24), thus allowing the phase of the signal to be determined from the data with no a priori assumptions about hemodynamic delay or impulse response function (higher-order harmonics are minimal for the short block duration used). A sigma filter was used to cluster pixels in a 3×3 region, as described previously (18). Activation maps were overlaid on the T_2 images for visual inspection.

The activation was quantitated using Kleinschmidt's method (25), which was implemented by choosing a region of interest (ROI) that included the cerebellum and pyriform cortex. The histogram of correlation coefficients in the ROI was calculated and smoothed. A normal distribution was fit to the central peak to determine the background and subtracted from the smoothed histogram to generate a new histogram of activated pixels in which the background distribution is nearly eliminated. A threshold of 0.2 in the correlation coefficient was used to determine activation for this distribution. The activation volume so determined was recorded for each of the six activation maps in terms of the number of voxels, and ratios were obtained to compare the spiral-in and spiral-in/out methods with the conventional spiral-out method. The ratios normalized for individual differences between subjects and scan plane orientations to provide accurate comparisons.

The activation amplitudes for activated voxels were also recorded, but were not used in the comparisons because the amplitudes were similar for all voxels in which signal was seen. Instead, the signal-to-noise ratio (SNR) was used as an additional measure for comparison of methods.

SNR

To compare noise sensitivity of the trajectories, the signal-to-fluctuation-noise ratio (SFNR) was obtained for the six time-series on each subject, by calculating an SFNR image as the time-series mean image divided by the standard deviation image (18). An ROI that covered most of the brain in a slice not compromised with SFG-induced dropout was chosen and fixed for all six SFNR images. As with the activation analysis, ratios were obtained to remove intersubject variations. Of particular interest was comparing the spiral-out trajectory with the spiral-in trajectory and the spiral-out portion of the combined trajectory to determine if the preceding spiral-in gradients induce additional noise.

RESULTS

The activation volumes and SFNR noise measurements for all subjects are listed in Table 1. The numbers in parentheses are normalized to corresponding values of activation volume and SFNR for the conventional spiral-out case to remove individual differences and coil differences. Figure 3 shows average spiral images as well as the corresponding activation maps for the spiral-out and spiral-in scans as well as the two combination images for one slice in subject 1. The spiral-in/out scans yielded similar results and are not shown. As is evident both qualitatively and quantitatively, the spiral-in technique performs substantially better than the spiral-out method in frontal-orbital regions. Furthermore, the combination of spiral-in and spiral-out images for the spiral-in/out acquisition yielded significantly improved activation over the conventional spiral-out trajectory. The noise measurements confirm that the combination of the two trajectories provides a substantial advantage in SNR in uniform brain. The weighted combination method performed better in the frontal-orbital regions than simple averaging in both the raw images and the activation. The SFNR values were not significantly different for the spiral-out acquisition and the spiral-out time-series from the spiral-in/out acquisition or for the

FIG. 3. T_2^*-weighted average images: (**a**) spiral-out and (**b**) spiral-in images from separate scans, (**c**) spiral-out image from a spiral-in/out trajectory, (**d**) simple average combination from a spiral-in/out scan, and (**e**) weighted combination from a spiral-in/out scan. Images from the spiral-in/out scan were similar to **a** and **b**, and are not shown.
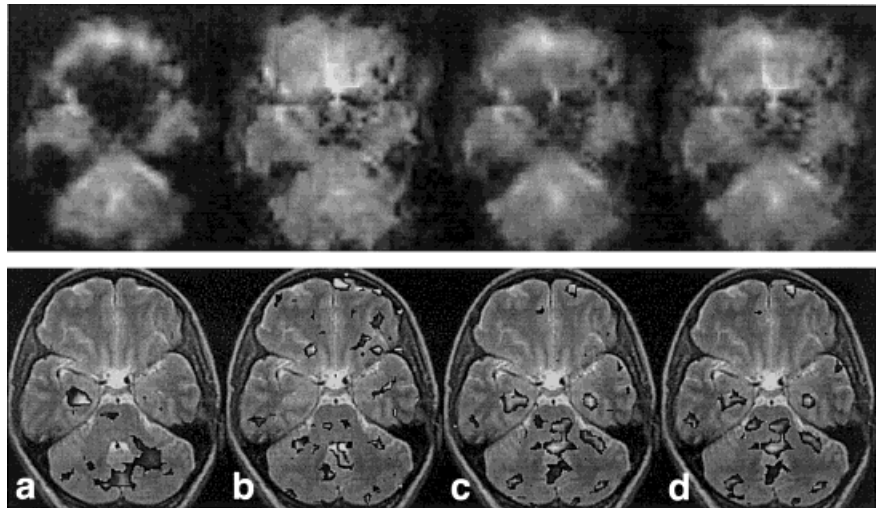
spiral-in acquisition, suggesting that the added gradient moments did not increase the brain motion sensitivity. Figure 4 shows T_2^*-weighted images for seven slices in a different subject, including spiral-out and spiral-in images from the separate scans, the spiral-out and -in images from the spiral-in/out acquisition and the combination image. Anatomic images are also provided for reference.

DISCUSSION

Functional imaging methods are hampered by the presence of SFGs which result in brain regions that can not be interrogated reliably by conventional rapid EPI or spiral acquisitions. This work has shown that spiral-in methods have advantages over spiral-out approaches in SFG-compromised regions, both in recovery of raw signal intensity and in BOLD contrast. The latter is an important result, because the trivial solution of reducing the TE will indeed reduce the signal dropout but also reduces the BOLD sensitivity.

The simulations assumed a transverse SFG with constant amplitude, which is patently simplistic. These results served only to demonstrate that such gradients could cause reduction of signal and BOLD contrast with spiral-
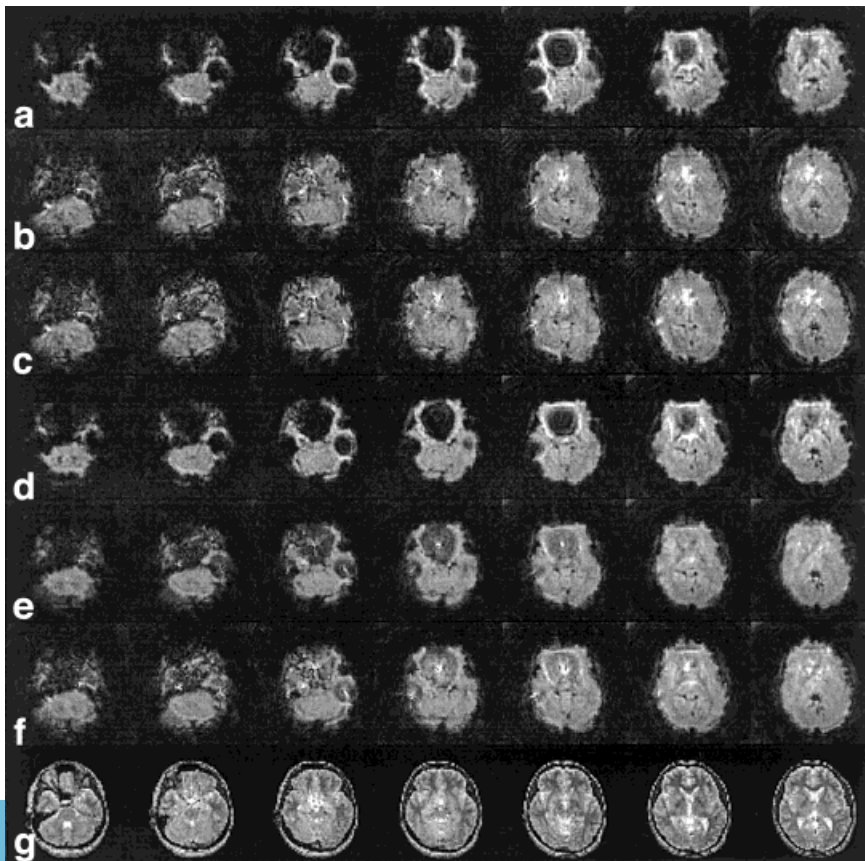

FIG. 4. Images from seven slices, showing (**a**) conventional spiral-out and (**b**) spiral-in scans, (**c**) spiral-in and (**d**) spiral-out images from spiral-in/out acquisition, (**e**) simple average of **c** and **d**, (**f**) weighted combination of **c** and **d** from spiral-in/out scan, (**g**) anatomic images. In SFG-compromised regions the weighted combination images recover the greatest signal.

out sequences, and that spiral-in trajectories could provide benefit. In reality, strong *z*-directed gradients are also established superior to the sinus and ear canals that play a role, as demonstrated by the *z*-shim approaches that recover signal by compensating for the *z*-directed gradient components (8). Thus, the experimentally observed increase in signal with the spiral-in trajectory demonstrates that signal recovery occurs even for highly complex field distributions (multidirectional gradients) near air cavities.

The SFNR is not significantly different for the spiral-in trajectory or for the spiral-out component of the spiral-in/out scan in comparison with the spiral-out trajectory, although there is a nonsignificant trend for a reduction in SFNR (0.98) for the latter, as shown in Table 1. This confirms that inclusion of the spiral-in trajectory before the spiral-out readout does not increase the latter's motion sensitivity. This differs from the results obtained by Bornert et al. (16) with multishot spiral-in trajectories, in which first-order moment compensation was required to reduce motion sensitivity. Perhaps the lack of motion sensitivity in our spiral-in and spiral-in/out scans resulted from having only one interleaf.

The results also confirm that the spiral-in/out trajectory provides an SNR advantage in uniform brain regions. The benefit (1.25 for the average or 1.3 for the weighted combination) is less than $\sqrt{2}$, as expected if the noise is correlated over a portion of the two readouts. This result is reasonable, given that a significant fraction of the image noise at 3T results from physiological fluctuations (4), which in turn implies a short-term correlation between the two acquisitions. The difference in SFNR between the two types of combinations of the spiral-in/out images was not significant in the uniform brain region used for these measurements, although inspection of Fig. 4 reveals obvious advantages for the weighted combination in the frontal areas.

The activation volumes are larger for the spiral-in acquisitions relative to the spiral-out scan, although there is considerable variability across subjects. The variations occur because of the severity of the SFG-induced dropout in the activation regions. The spiral-out activation in the spiral-in/out scan shows anomalously higher activation for several subjects and none for one subject, but the differences are not significant. The combination images have significantly greater activation than the spiral-out scan ($3.97\times$ for the simple average), and there is a nonsignificant trend for the weighted combination to excel over the simple average ($4.18\times$).

The spiral-in and spiral-out trajectories investigated here have the same TE, defined as the time at which the origin of *k*-space is sampled. However, the highest spatial frequencies are sampled with substantially different T_2^* decay times for the two trajectories (2 Tad). In brain areas with large SFGs the signal is essentially null at the TE, so the spiral-out image shows a signal void. In such regions, the spiral-in image intensity derives only from sampling by the higher spatial frequencies. Thus, even though image intensity is recovered in this image, its BOLD sensitivity is reduced (as shown in Fig. 2d, for example). Moreover, the severe filtering of the lower spatial frequencies will affect the contrast by amounts that depend on the size of the activation regions. However, activation regions that are small relative to the FOV (which is frequently the case) have a broad *k*-space spectrum and are affected less than the raw brain signal.

The use of activation volumes can be questioned as a metric for comparison. In the past, both volumes and activation signal amplitude have been used. In this case, the number of activated voxels is much greater with the methods that include the spiral-in trajectory, whereas the SFNR is comparable and thus the volumes make the most sense. However, the issue could be compounded by the difference in spatial frequency weighting of the spiral-in and spiral-out trajectories, which (as stated above) could affect the spatial impulse response function and therefore both the amplitude and spatial extent of activation signal in SFG-compromised regions. Therefore, the comparison should not be construed as rigorously quantitative.

The maps in Fig. 3c (simple average) and d (weighted average) are nearly identical because little additional signal was derived in the activated regions from the spiral-out component. It could be argued that the additional signal in the combined images does not actually provide increased BOLD activation. However, Fig. 2 shows that it is possible to recover BOLD contrast. Moreover, off-resonance acquisition with spiral trajectories does not result in significant displacement of the signal, so signal observed in a given voxel derived from tissue in that location. In many cases, the adaptively combined images have greater signal, as in the more inferior slices in Fig. 4e and f. However, in some slices (such as slice 5 in Fig. 4) the spiral-out image has a bright ring around its signal void, which remains prominent in the combined images. This ring results from rapid changes in the frequency accompanied by blurring and could be misleading in the combined images. This would be easily discriminated in the combination, if desired.

While the spiral-in/out results are encouraging, several areas require additional exploration. The weighted combination results (Fig. 3c,d and Fig. 4e,f) demonstrate that adaptive combination methods may give better results in nonuniform regions in which the spiral-out image gives little signal. Other techniques that use combinations in either raw image space or after some form of activation analysis (26) may provide even greater benefit. Another area for investigation is examining parameter choices for the spiral-in/out trajectory, which could include nonuniform density of *k*-space coverage, especially between the spiral-in and spiral-out portions.

Finally, the spiral-in/out trajectory is similar to the single-shot EPI trajectory in that redundant *k*-space coverage is obtained before and after TE. In the case of EPI, the combination of the data occurs during reconstruction of one image, while with the spiral-in/out method the combination can be performed adaptively from two images. This suggests that EPI acquisitions in SFG regions may benefit if two magnitude images are separately reconstructed from the data before and after TE using a partial *k*-space algorithm and combined adaptively. One difference between EPI and the spiral-in/out trajectory is that while each half of the spiral readout is shorter than a complete EPI trajectory due to improved efficiency of the spiral, the total duration is longer.

In summary, the spiral-in trajectory recovers increased signal and BOLD contrast in regions where signal is tradi-

tionally lost due to SFGs. The novel spiral-in/out trajectory provides substantially increased SNR in uniform brain regions and retains signal in SFG-compromised regions when an adaptive combination of the spiral-in and spiral-out images is used. Some caution is warranted because the recovered signal is severely filtered in those regions by susceptibility-induced decay, with high spatial frequencies accentuated. Nevertheless, the spiral-in/out trajectory may be advantageous for many studies of cognitive function.

ACKNOWLEDGMENTS

APPENDIX

Derivation of Signal for Spiral-In and Spiral-Out Trajectories

A general object is assumed to have spatial intensity distribution $\rho(\mathbf{r})$, where $\mathbf{r}$ denotes a 2D spatial variable. Furthermore, assume there is a dephasing SFG with field distribution $b(\mathbf{r})$. Then the measured signal $S(t)$ during a spiral-out readout with trajectory defined by $\mathbf{k}(t) \equiv k_x(t)\, \mathbf{a}_x + i\, k_y(t)\, \mathbf{a}_y$, where $0 \leq t \leq Tad$, is:

$$S(t) = \int_{-D/2}^{D/2} \rho(\mathbf{r}) e^{i\mathbf{k}(t)\cdot\mathbf{r}} e^{-[i\gamma b(\mathbf{r}) + R_2^*](TE \pm t)}\, d\mathbf{r}, \qquad [\text{A1}]$$

where D is the FOV, the positive sign is chosen for spiral-out and negative sign for spiral-in trajectories, $R_2^* = 1/T_2^*(\mathbf{r})$, γ is the gyromagnetic ratio for protons and $(\mathbf{a}_x, \mathbf{a}_y)$ are unit vectors. The reconstruction is given by

$$I(r) = \frac{1}{Tad} \int_0^{Tad} S(t) e^{-i\mathbf{k}(t)\cdot\mathbf{r}} \left|\frac{\partial k}{\partial t}\right| dt. \qquad [\text{A2}]$$

In order to evaluate Eqs. [A1] and [A2] it is necessary to consider a specific case. Assume for simplicity the object has homogeneous R_2^* and Gaussian shape, and is centered at the origin, so that

$$\rho(\mathbf{r}) = \frac{1}{\pi a^2} e^{-(x^2 + y^2)/a^2}. \qquad [\text{A3}]$$

Furthermore, assume the SFG is directed only along the x axis with linear gradient amplitude g, so that b = g x. The single shot spiral trajectory can be well approximated by the slew rate limited formulation (19)

$$\mathbf{k}(t) = \alpha t^{2/3}[\cos(\beta t^{2/3})\mathbf{a}_x + i \sin(\beta t^{2/3})\mathbf{a}_y], \qquad [\text{A4}]$$

where $\alpha = \pi / (p\ Tad^{2/3})$, $\beta = D\ \alpha$, and p is the pixel size $\equiv$ D/N. Then, Eq. [1] becomes

$$S(t) = e^{-(TE \pm t)R_2^*} e^{-(q_x^2 + q_y^2)a^2/4}, \qquad [\text{A5}]$$

where $q_x = k_x + \gamma g (TE \pm t)$, $q_y = k_y$.

It is sufficient to consider the reconstructed image intensity at the origin for demonstration purposes. From Eqs. [2] and [5], this is given by

$$I_0 = |I(0)| = \left| \frac{1}{Tad} \int_0^{Tad} S(t) \left|\frac{\partial k}{\partial t}\right| dt \right|$$

$$= e^{-TE\,R_2^*} \left| \int_0^1 e^{\mp \tau R_2^* Tad} e^{iN\pi\tau^{2/3}} e^{-(q_x^2 + q_y^2)a^2/4} \tau^{1/3}\, d\tau \right|,$$

$$\equiv e^{-TE\,R_2^*} \left| \int_0^1 Q_{\pm}(\tau)\, d\tau \right| \qquad [\text{A6}]$$

which defines $Q_{\pm}(\tau)$.

REFERENCES

1. Ogawa S, Lee TM, Kay AR, Tank DW. Brain magnetic resonance imaging with contrast dependent on blood oxygenation. Proc Natl Acad Sci USA 1990;87:9868–9872.
2. Ogawa S, Tank DW, Menon R, Ellermann JM, Kim SG, Merkle H, Ugurbil K. Intrinsic signal changes accompanying sensory stimulation: functional brain mapping with magnetic resonance imaging. Proc Natl Acad Sci USA 1992;89:5951–5955.
3. Wansapura JP, Holland SK, Dunn RS, Ball Jr WS. NMR relaxation times in the human brain at 3.0 tesla. J Magn Reson Imaging 1999; 9:531–538.
4. Kruger G, Kastrup A, Glover G. Neuroimaging at 1.5T and 3.0T: comparison of oxygen-sensitive magnetic resonance imaging. Magn Reson Med 2000;45:595–604.
5. Frahm J, Merboldt KD, Hanicke W. The influence of the slice-selection gradient on functional MRI of human brain activation. J Magn Reson B 1994;103:91–93.
6. Constable R, Spencer D. Composite image formation in Z-shimmed functional MR imaging. Magn Reson Med 1999;42:110–117.
7. Yang QX, Dardzinski BJ, Li S, Eslinger PJ, Smith MB. Multi-gradient echo with susceptibility inhomogeneity compensation (MGESIC): demonstration of fMRI in the olfactory cortex at 3.0 T. Magn Reson Med 1997;37:331–335.
8. Yang QX, Williams GD, Demeure RJ, Mosher TJ, Smith MB. Removal of local field gradient artifacts in T2*-weighted images at high fields by gradient-echo slice excitation profile imaging. Magn Reson Med 1998; 39:402–409.
9. Glover G. 3D z-shim method for reduction of susceptibility effects in BOLD fMRI. Magn Reson Med 1999;42:290–299.
10. Lai S, Glover G. Three-dimensional spiral fMRI technique: a comparison with 2D spiral acquisition. Magn Reson Med 1998;39:68–78.
11. Merboldt KD, Finsterbusch J, Frahm J. Reducing inhomogeneity artifacts in functional MRI of human brain activation-thin sections vs gradient compensation. J Magn Reson 2000;145:184–191.
12. Cho ZH, Ro YM. Reduction of susceptibility artifact in gradient-echo imaging. Magn Reson Med 1992;23:193–200.
13. Glover G, Lai S. Reduction of susceptibility effects in BOLD fMRI using tailored RF pulses. In: Proceedings of the 6th Annual Meeting of ISMRM, Sydney, Australia, 1998. p 298.
14. Stenger VA, Boada FE, Noll DC. Three-dimensional tailored RF pulses for the reduction of susceptibility artifacts in T2*-weighted functional MRI. Magn Reson Med 2000;44:525–531.

15. Noll D, Cohen J, Meyer C, Schneider W. Spiral k-space MR imaging of cortical activation. J Magn Reson Imaging 1995;5:49–57.
16. Bornert P, Aldefeld B, Eggers H. Reversed spiral MR imaging. Magn Reson Med 2000;44:479–484.
17. Farzaneh F, Riederer SJ, Pelc NJ. Analysis of T2 limitations and off-resonance effects on spatial resolution and artifacts in echo-planar imaging. Magn Reson Med 1990;14:123–139.
18. Glover GH, Lai S. Self-navigated spiral fMRI: interleaved versus single-shot. Magn Reson Med 1998;39:361–368.
19. G. Glover G. Simple analytic spiral k-space algorithm. Magn Reson Med 1999;42:412–415.
20. Sobel N, Prabhakaran V, Desmond JE, Glover GH, Goode RL, Sullivan EV, Gabrieli JD. Sniffing and smelling: separate subsystems in the human olfactory cortex. Nature 1998;392:282–286.
21. Kim DH, Adalsteinsson E, Glover G, Spielman S. SVD regularization algorithm for improved high-order shimming. In: Proceedings of the 8th Annual Meeting of ISMRM, Denver, 2000. p 1685.
22. Duyn JH, Yang Y, Frank JA, van der Veen JW. Simple correction method for k-space trajectory deviations in MRI. J Magn Reson 1998;132:150–153.
23. King KF, Ganin A, Zhou XJ, Bernstein MA. Concomitant gradient field effects in spiral scans. Magn Reson Med 1999;41:103–112.
24. Lee AT, Glover GH. Discrimination of large venous vessels in time-course spiral blood oxygen dependent magnetic resonance functional neuroimaging. Magn Reson Med 1995;33:745–754.
25. Kleinschmidt A, Requardt M, Merboldt K, Frahm J. On the use of temporal correlation coefficients for magnetic resonance mapping of functional brain activation. Individualized thresholds and spatial response delineation. Int J Imaging Syst Technol 1995;6:238–244.
26. Posse S, Wiese S, Gembris D, Mathiak K, Kessler C, Grosse-Ruyken ML, Elghahwagi B, Richards T, Dager SR, Kiselev VG. Enhancement of BOLD-contrast sensitivity by single-shot multi-echo functional MR imaging. Magn Reson Med 1999;42:87–97.